From Planar Boron Clusters to Borophenes and Borospherenes

Lai-Sheng Wang*

Department of Chemistry, Brown University, Providence, Rhode Island 02912, USA

*E-mail: Lai-Sheng_Wang@brown.edu

Abstract

Photoelectron spectroscopy in combination with computational chemistry has been used over the past decade to systematically elucidate the structures and chemical bonding of size-selected boron clusters. Small boron clusters have been found to be planar or quasi-planar with both delocalized σ and π bonding. A particularly interesting cluster is B_{36}, which has been found to possess a planar structure with a central hexagonal vacancy. The hexagonal B_{36} can be viewed as a repeating unit to assemble atom-thin boron monolayers (dubbed borophenes). This finding provides the first indirect experimental evidence that borophenes with hexagonal vacancies are potentially viable. Another exciting discovery has been the observation and characterization of the first all-boron fullerenes. Photoelectron spectroscopy revealed that the B_{40}^- cluster consisted of two isomers with very different electron binding energies. Global minimum searches led to two nearly degenerate isomers competing for the global minimum: a quasi-planar isomer and an unprecedented cage isomer. In the neutral, the B_{40} cage is overwhelmingly the global minimum, which is the first all-boron fullerene to be observed and is named "borospherene". There is evidence that there exists a family of borospherenes with B_{28} being the smallest borospherene. It is expected that the pace of discovery will continue to accelerate in boron clusters, and more interesting structures and chemical bonds will be uncovered with heightened research interests and more sophisticated experimental and computational methods.

International Symposium on Clusters and Nanomaterials, edited by Puru Jena, Anil K. Kandalam, Proc. of SPIE Vol. 10174, 1017402 · © 2016 SPIE
CCC code: 0277-786X/16/$18 · doi: 10.1117/12.2254384

1. Introduction

Ever since the discoveries of fullerenes and carbon nanotubes, there have been interests about whether other elements can form similar structures. Boron is the most promising element because of the strong boron-boron bonds as reflected by the fact that bulk boron has the highest melting temperature second only to carbon among the main group elements. Indeed, both boron-based nanotubes and fullerene-like cages have been considered computationally [1-5]. But their viability requires systematic understanding about the structures and bonding of small boron clusters and their evolution as a function of size.

There were scarce experimental studies on boron clusters before 2000 [6-10]. Since then, photoelectron spectroscopy (PES), in conjunction with theoretical calculations, has been used to probe the electronic structure and chemical bonding of size-selected boron clusters [11-18], whereas ion mobility has been used to probe the structures of cationic boron clusters [19]. The structures and bonding of boron cluster anions (B_n^-) with up to 27 atoms have been systematically elucidated and all found to have planar or quasi-planar (2D) global minimum structures [20-27]. Since size-selection by mass spectrometry requires charged clusters, negatively-charged boron clusters have been the main focus in the PES studies and global minimum searches [28]. All 2D boron clusters consist of a periphery and one or more interior boron atoms. Chemical bonding analyses found that all peripheral boron atoms are bonded by classical 2-center-2-electron (2c-2e) bonds, whereas the interior atoms are bonded by delocalized bonds [18,28-31], as a result of boron's electron deficiency. There are both delocalized σ and π bonds in 2D boron clusters, giving rise to the concept of multiple aromaticity. The π systems of the 2D boron clusters are found to obey the Huckel rule and analogy with polycyclic aromatic hydrocarbons (PAHs) has been found for most aromatic boron clusters [14,15,28].

In particular, the discovery of the planar hexagonal B_{36} cluster and its implication for the viability of borophenes [32] and the discovery of the first all-boron fullerene (borospherene) at B_{40} [33] have stimulated considerable recent interests in boron clusters and nanostructures. An extensive review was published by Alexandrova et al. for the studies of boron clusters reported

before 2005 [18]. A brief account of the unique bonding and structural characteristics of planar boron clusters has also appeared by Sergeeva et al. [29], as well as the aromatic properties of planar boron clusters [34]. Very recently, a more comprehensive review for the progress made over the past ten years using PES in conjunction with computational chemistry, has been published [28]. The current article highlight a few major advances that led to the discoveries of borophenes and borospherenes and provides some personal perspectives.

2. Structures and PES of medium-sized boron clusters, B_n^- (n = 3–27)

Figure 1 summarizes the global minimum structures of B_n^- for n = 3 to 27. Isomers have been observed for some clusters, but only those for the two largest clusters (B_{25}^- and B_{27}^-) in this size range are included in Figure 1 [26,27]. It should be noted that a new isomer has been found for B_9^- [35], in addition to the beautiful D_{8h} global minimum molecular wheel reported in the original study [14]. Some of the 2D structures shown in Figure 1 are quasi-planar. For example, both B_7^- and B_{12}^- were found to have bowl-shaped structures [15,16], even though both were aromatic. The out-of-plane distortion was found to be due to the fact that the peripheral B–B bonds were stronger with slightly shorter bond lengths and could squeeze out the interior atoms slightly. This observation was confirmed by substituting a peripheral B atom by a larger valence-isoelectronic Al atom and the resulting AlB_6^- and AlB_{11}^- clusters were found to be planar [36].

Neutral boron clusters are considerably more challenging to study. The infrared (IR) spectrum of neutral B_{11} was obtained using an IR/UV two color ionization scheme in the wavelength range from 650 to 1550 cm^{-1} [37]. It was found that the global minimum of neutral B_{11} (C_{2v}, $^2B_2$) is nearly identical to that of the B_{11}^- anion (Figure 1) [15]. A more significant experimental study was carried out by Oger et al. to probe the B_n^+ cation structures for n = 12–25 using ion mobility in combination with DFT calculations [19]. The structures of B_{12}^+ and B_{15}^+ were found to be similar to those of the corresponding anions (Figure 1), whereas the structures of B_{13}^+ and B_{14}^+ were found to be more circular, consistent with previous calculations [38].

Because of the enormous challenges of global minimum searches, progress was very slow in solving the structures of boron clusters beyond 15 atoms, except B_{20}^- [17]. Preliminary photoelectron data were obtained for B_n^- up to $n = 42$ around 2005, as shown in Figure 2, which displays a manual plot about the trend of the estimated first adiabatic electron detachment energies (ADEs) of B_n^- or the electron affinity (EA) of the corresponding neutral B_n clusters as a function of cluster size for $n = 3–42$. To this day, not all clusters in this size range have been solved. Precise EAs and the first vertical electron detachment energies (VDEs) for those clusters that have been published are summarized in ref. 28. The EAs in Figure 2 are approximate values for $n = 16–19$ and 21–42 estimated from the preliminary photoelectron spectra. Even with the approximate values, Figure 2 clearly showed odd-even alternations for $n > 8$, indicating that all odd-sized B_n^- anions are closed shell and the even-sized B_n neutral clusters are closed shell. Specifically, note was taken for the two unusual data points at $n = 36$ and 40, that foresaw future discoveries for borophenes [32] and borospherenes [33]. With increasing powers in computational hardware and software, much faster progress has been possible since 2011.

After the B_{20}^- cluster was solved in 2005 [17], the structures between B_{16}^- to B_{19}^- were solved [20-22] and it took seven years to solve the next larger cluster, B_{21}^- [23]. In addition to the challenges of global minimum searches, the photoelectron spectrum of B_{21}^- was very congested, making it difficult to compare with calculations and posing much more demands on the accuracy of the calculations. To guarantee a more thorough global minimum search, a more efficient method, called Cartesian Walk (CW) [23], was developed by Piazza in the Wang group in collaboration with the Boldyrev group. CW was made to rapidly search for 2D structures, though it could also search for 3D structures. The CW global search method was essential to allow the structures from B_{21}^- to B_{27}^- to be systematically solved [28]. All these clusters are found to be 2D, as shown in Figure 1.

3. The structure of B36 and the implications for Borophenes

The preliminary Figure 2 showed that the B_{36}^- cluster had an unusually low electron binding energy, suggesting that it might have an interesting structure with high symmetry. However, for several years it could not be solved because of the challenges of global minimum searches. With the increasing computational power and the development of the CW global minimum search method, a breakthrough was made in 2013 to solve the structures of B_{36}^- and B_{36} [32]. Their quasi-planar hexagonal global minima with a central hexagonal hole were quite surprising. Upon solving B_{36}^-, the solutions of several mid-sized boron clusters were quickly followed [39-41], including the even more surprising B_{40} borospherene [33].

3.1. *Photoelectron spectroscopy and comparison with theoretical calculations*

The photoelectron spectrum of B_{36}^- at 193 nm is shown in Figure 3, revealing anomalously low electron binding energies [32]. The ground state band (X) yielded a first VDE of 3.3(1) eV and an ADE of 3.12(3) eV. The ADE also represented the EA of neutral B_{36}, and it was lower than that of all the smaller clusters above B_{20} (Figure 2). The global minimum of B_{36}^- was first searched using the CW method. Among roughly 500 trial structures, a quasi-planar structure with near C_{6v} symmetry and a central hexagonal hole was found to be the lowest energy structure. To confirm this result, the global minimum was further searched using a constrained basin-hopping method, called TMmin, developed in Jun Li's group at Tsinghua University [32]. Among the approximately 2,500 structures generated by TGmin, again a pseudo-C_{6v} B_{36}^- was found to be the global minimum, consistent with the CW search. The global minimum and two low-lying isomers of B_{36}^- are shown in Figure 4a. The global minimum of B_{36}^- actually had C_{2v} symmetry with a doublet electronic state ($^2A_1$), slightly distorted from the perfectly hexagonal C_{6v} symmetry. At the PEB0 level of theory, the second isomer had a tubular or triple-ring structure and the third isomer was 2D with a hexagonal and a heptagonal double hole. At the higher CCSD level, the 2D isomer III was only 1.17 kcal/mol above the global minimum, whereas the tubular isomer II was much higher in energy, being 23.97 kcal/mol above the global minimum. For neutral B_{36}, the structures of the anions by removing an electron were optimized at

the PBE0 level of theory. The hexagonal global minimum became perfectly C_{6v} symmetry with a close-shell electronic configuration (I^0 in Figure 4b). The tubular and the double-hole 2D isomer were at least 20 kcal/mol higher in energy.

The simulated photoelectron spectra of isomers I to III are compared with the experimental spectrum in Figure 3. The simulated spectrum of isomer I was in excellent agreement with the experiment, providing unequivocal evidence for the hexagonal global minimum for B_{36}^-. The simulated spectrum of the tubular isomer II did not agree with the experiment. On the bases of both the simulated spectrum and the energetics, the tubular structure could be ruled out. If the CCSD energy was reliable, the double-hole 2D isomer III should be accessible experimentally. The simulated spectrum of isomer III would be overlapped with the features of the dominating global minimum. The weak X' feature was in good agreement with the first calculated VDE of isomer III and could be taken as experimental evidence for the population of the double hole 2D isomer, which was quite interesting on its own right, though in the neutral this isomer was much higher in energy at the PBE0 level (III^0 in Figure 4b).

3.2. *The implication of the hexagonal B_{36} for the viability of borophenes*

Because of its electron deficiency, boron cannot form hexagonal layers like graphene. By filling a boron atom to the center of the hexagon in a graphene-like structure, one obtains a boron sheet with a triangular lattice, which has been considered for boron nanotubes [1,2]. However, such a triangular lattice is too electron-rich and out-of-plane distortions occur, giving rise to a rippled boron layer [42-45]. It was proposed via DFT calculations that a triangular lattice with periodic hexagonal holes was much more stable than a close-packed triangular lattice [3,4]. More importantly, such a structure was perfectly planar and would be better to form boron nanotubes [4,46].

The hexagonal hole in the B_{36} cluster is reminiscent of the hexagonal holes in the 2D boron sheets [3,4]. The B_{36} cluster can be viewed as the analogous boron unit of the hexagonal C_6 unit in graphene to form extended graphene-like monolayer boron nanostructures with

hexagonal holes, as shown schematically in Figure 5. The structure shown in Figure 5 represented a hexagonal hole density of $\eta = 1/27$ (one vacancy per 27 lattice sites in a triangular lattice), as defined for the 2D boron sheet [3]. The structure in Figure 5 was constructed by sharing a row of B atoms between two neighboring B_{36} units. The apex atoms (circled in Figure 5) were shared by three neighboring B_{36} units. If these atoms were removed, one arrived at the more stable α-sheet with $\eta = 1/9$ [3,4]. A B_{30} model cluster was used to analyze the bonding in the proposed α-sheet [47], which was equivalent to removing all six apex B atoms in the B_{36} cluster. Hence, it was suggested that the B_{36} cluster could be viewed as the embryo for the proposed stable 2D boron sheets. More importantly, the hexagonal B_{36} cluster provided indirect evidence for the viability of monolayer borons with hexagonal vacancies. A name "borophene" was, thus, coined to designate this class of new boron nanostructures [32].

Several theoretical studies on large boron clusters have appeared recently, reporting 2D structures with various arrangements of hexagonal holes. Xu *at al*. investigated B_n (n = 30–51) and found a stable planar B_{49} cluster with a double-hexagonal vacancy [48]. Kumar and co-workers studied the B_{84} cluster and found a quasi-planar structure with four hexagonal holes [49]. This 2D structure was shown to be more stable than various tubular structures containing hexagonal holes.

It should be pointed out that Figure 5 was only schematically showing the relationship between the B_{36} cluster with a hexagonal hole and the putative borophenes. It did not represent the growth mechanism of borophenes. Because bulk boron does not have a layered structure, it would be difficult to achieve free-standing borophenes. It is likely that borophene would have to be grown on relatively inert substrates. It was suggested computationally that coinage metals would be suitable substrates for borophenes or they may be formed on surfaces of metal borides [50-52]. Thus, B_{36} or other small boron clusters with hexagonal holes may serve as the nucleus for the formation of large-scale borophenes on surfaces. Very recently, two reports have appeared about the syntheses of borophenes on silver surfaces using atomic deposition and high-resolution STM studies [53,54]. Even though Mannix et al. suggested that their borophene has a

buckled triangular structure [53], Feng et al. reported borophenes with the expected hexagonal holes synthesized using a similar atomic deposition method on a silver substrate [54]. The conclusions by Feng et al. are supported by a subsequent computational studies [55].

3.3. *B_{35}^-: A more flexible motif for borophenes*

The photoelectron spectrum of B_{35}^- at 193 nm shown in Figure 6a was well resolved and appeared relatively simple [40], suggesting that there were likely no mixtures of low-lying isomers. The B_{35}^- spectrum displayed some resemblance to the high binding energy part of the B_{36}^- spectrum minus the X band (Figure 3a). This observation hinted that the structure of B_{35}^- might be similar to B_{36}^-. Global minimum searches led to a structure of B_{35}^- with a double-hexagonal vacancy (DHV), as shown in Figure 7. The global minimum of B_{35}^- was quasi-planar with a closed shell electronic structure ($^1A'$). The next lowest-lying isomer was in fact a triplet state of the same structure at 12 kcal/mol above the global minimum singlet state at the PBE0 level of theory. All other isomers were at least 14 kcal/mol higher in energy above the global minimum, suggesting the overwhelming stability of the DHV structure for B_{35}^-. The simulated spectrum of the DHV global minimum of B_{35}^- is compared with the experiment in Figure 6b. The agreement with the experiment was almost quantitative, providing firm confirmation of the stability of the DHV global minimum for B_{35}^-. The excellent agreement between experiment and theory also indicated that there was no population of low-lying isomers experimentally.

The DHV global minimum of B_{35}^- could be viewed as removing an atom from the hexagonal B_{36}^- cluster with little structural relaxation. In fact, the DHV structure of B_{35}^- could be overlaid on top of the hexagonal B_{36}^- global minimum, consistent with the PES similarity of the two clusters. The central hexagonal hole in the C_{6v} B_{36} was critical for its 2D structure. The slight out-of-plane distortion was really due to the peripheral effect, i.e., the peripheral B–B bonds tend to be stronger or slightly shorter than the interior B–B bonds. It was interesting to note that the second hexagonal hole in B_{35}^- induced very little structural distortion and in fact made the cluster slightly more planar, reinforcing the importance of hexagonal vacancies in the stabilization of

borophenes. The hexagonal B_{36} cluster was considered as a motif for borophene consisting of isolated hexagonal holes or the α-sheet (Figure 5). Other monolayer boron sheets were also considered theoretically with different hexagonal hole density and patterns [56,57]. For example, the so-called β-sheet referred to boron monolayers with DHVs or adjacent hexagonal holes [3]. It was found that the planar B_{35} cluster was in fact a more flexible motif to construct borophenes with DHVs or mixed hexagonal holes and DHVs. Figure 8 shows schematically two such arrangements [40]. Other arrangements of the B_{35} clusters would be possible, allowing the creation of borophenes with different hole densities.

A careful examination of Figure 1 shows that many small boron clusters display tetragonal and pentagonal defects. B_{27}^- was the smallest boron cluster with a hexagonal defect among its most stable isomers [27]. Between B_{27}^- and B_{35}^-, only B_{30}^- has been experimentally studied and its global minimum also contains a hexagonal hole [39]. Hence, it seems that the hexagonal hole, which is critical for truly planar borophenes, may be a common feature in large 2D boron clusters.

4. All-boron cage clusters: Borospherenes

In addition to the unusually low EA for B_{36}, the preliminary Figure 2 showed that B_{40} had an even lower EA, suggesting a very stable electronic system for this cluster. Over the years, several structures were tested, mainly the tubular types, but none agreed with the experiment. The 40-atom boron cluster was finally solved after the solution of B_{36} as a result of new global minimum search methods and increased computer powers through a multi-way experimental and theoretical collaborative effort [33].

4.1. *B_{40}^- and B_{40}: The first all-boron fullerene – borospherene*

The photoelectron spectrum of B_{40}^- at 193 nm is shown in Figure 9 [33]. The weak X' peak defined a very low EA of 2.50 eV for B_{40}, as indicated in Figure 2. The weak intensity of this peak suggested that it might come from a weakly populated isomer, whereas the X band

might represent the ground state transition for the main isomer of the B_{40}^- anion. The global minimum of B_{40}^- was searched using two methods independently, the TGmin code [32] and the stochastic surface walking (SSW) method [58]. A total of 5,300 structures were searched for B_{40}^- by TGmin and 3,565 structures by SSW. Similar searches were performed for neutral B_{40} using TGmin and SSW. Figure 10 displays the configurational energy spectra within 1.5 eV of the global minimum for both B_{40}^- and B_{40} at the PBE0 level of theory. The structures of the global minima and selected isomers are given. In general, three types of structures were found: quasi-planar, 3D cage, and tubular structures (Figure 10a). The global minimum of B_{40}^- was a quasi-planar structure with a DHV, similar to that of B_{35}^- (Figure 7). Most interestingly, the second isomer of B_{40}^- was a cage structure only 0.1 eV above the DHV planar global minimum. The third isomer was a quasi-planar structure, similar to B_{36}^- (Figure 4). The fourth isomer was also a cage structure, while the fifth isomer was planar, featuring a heptagon. B_{40}^- was the first boron cluster, where a heptagonal hole appeared in a low-lying 2D isomer.

The simulated spectrum of the DHV global minimum of B_{40}^- was compared with the experiment in Figure 9b. The DHV global minimum gave very high electron binding energies and its simulated spectrum was in good agreement with the intense PES features (X, A–D). The cage isomer was very close to the DHV global minimum in energy and could be populated experimentally. The simulated spectrum of the cage structure was shown in Figure 10c. The cage structure exhibited a very large HOMO-LUMO gap and a very low electron binding energy for its first detachment feature, in excellent agreement with the weak PES band (X') at the low binding energy side. The higher binding energy detachment features of the cage isomer overlapped with the PES bands of the DHV global minimum. The combination of the two lowest-energy isomers was in perfect agreement with the experiment, providing considerable credence for the global minimum of B_{40}^- and its low-lying cage isomer.

There was a re-ordering of the different isomers in neutral B_{40} (Figure 10b). In the neutral, the cage structure was the global minimum and was overwhelmingly stable. The next lowest-lying isomer of B_{40} was also a cage 0.5 eV higher in energy, whereas the DHV isomer

was about 1 eV higher in energy in the neutral. The detailed structures of the DHV global minimum and the cage isomer are shown in Figure 11 for both the anion and the neutral B_{40}. There was relatively little structural change between the anions and the neutrals of the two isomers. The DHV isomer had C_s symmetry with a slight bowl shape.

The cage structure had D_{2d} symmetry, with two hexagons, four heptagons, and forty-eight B_3 triangles. The cage structure was unprecedented for boron clusters. Even though a B_{80} cage was suggested computationally previously [5], subsequent calculations showed that it was energetically unfavorable in comparison with other low-symmetry more closed packed structures [59-62]. The B_{40} cage had a diameter of 6.2 Å, compared to the 7.1 Å diameter for the fullerene C_{60} [63]. The B_{40}^- cage was the first all-boron fullerene to be observed and characterized experimentally. A name, "borospherene", was coined for the all-boron fullerene [33].

4.2. *B_{39}^-: A chiral borospherene*

The photoelectron spectrum of B_{39}^-, shown in Figure 12a at 193 nm, was quite complicated, posing considerable challenges for comparison with theory. Its electron binding energies were significantly higher than that of B_{40}^-. The spectrum was congested with numerous unresolved features, suggesting the possibility of co-exiting isomers in the cluster beam. Global minimum searches for B_{39}^- were done using the minimum-hopping [64] and TGmin methods independently. Initial structures for the minimum-hopping searches were primarily based on the B_{40} cage structure by removing one boron atom from different positions of the borospherene surface, as well as manual structural constructions. About 5,000 isomers were found from eight independent minimum-hopping searches. Many cage-like structures were found to be among the low-lying isomers, along with 2D and tubular type isomers. More than 4,600 isomers were produced independently using the TGmin code [32]. The low-lying isomers within 0.5 eV of the global minimum are shown in Figure 13 at the CCSD(T) level of theory.

Figure 14 shows in more detail the global minimum C_3 cage structure of B_{39}^- at the CCSD(T) level and the second lowest-lying C_2 cage isomer, which is only 0.08 eV above the C_3

isomer. It was found that both the C_3 and C_2 cage isomers were axially chiral and their enantiomers are also shown in Figure 14, where the hexagonal and heptagonal rings are shaded for better structural viewing. The degenerate global minima C_3(**1**) and C_3(**1'**) formed a pair of axially chiral enantiomers with respect to the C_3 symmetry axis; the C_2(**2**) and C_2(**2'**) isomers formed a pair of axially chiral enantiomers about the C_2 symmetry axis. Among the first ten most stable isomers at the CCSD(T) level (Figure 13), there were five additional low-symmetry cages: C_1(**3**), C_1(**5**), C_1(**6**), C_2(**8**), and C_1(**10**), which were all chiral in nature. The first non-cage isomer had a slightly distorted tubular structure (**4** in Figure 13). The first quasi-planar isomer (**7**, C_s) was 0.28 eV above the global minimum at CCSD(T) and it was similar to the hexagonal B_{36}^- cluster by attaching three B atoms along one edge (Figure 4). Another quasi-planar isomer (**9**, C_s) had a central heptagonal hole.

The simulated spectrum for the C_3 global minimum was compared with the experiment in Figure 12b and was in agreement with some of the observed features. Clearly, other isomers must be populated experimentally and contributed to the observed spectrum. The simulated spectrum of the low-lying C_2 isomer is shown in Figure 12c. The combination of the two isomers agreed well with the experiment and explained the complexity of the observed photoelectron spectrum.

The structure and bonding of the chiral C_3(**1**) and C_2(**2**) cage structures of B_{39}^- were related to those of the B_{40} borospherene. The C_3(**1**) B_{39}^- could be constructed from the B_{40} cage by replacing a B_7 heptagon with a B_6 hexagon, followed by a structural rearrangement. Hence, the C_3 cage consisted of three heptagons on the top half and three hexagons on the bottom half, as well as forty-seven triangles. The C_2(**2**) B_{39}^- cage could be obtained from the B_{40} borospherene by removal of one B atom on the waist, so that one of the boron double chain on the waist was narrowed to a single atom to cause a "defect" site (**2** in Figure 14). Thus, the C_2 cage had the same numbers of hexagons and heptagons as the B_{40} borospherene, as well as forty-six triangles.

Chen et al. reported recently a computational study of B_{41}^+ and B_{42}^{2+} and found that these boron cluster cations had cage structures with π bonding patterns also similar to the B_{40}

borospherene [65]. The B_{41}^+ borospherene had C_1 symmetry and the B_{42}^{2+} borospherene had C_2 symmetry. Hence, both were chiral like B_{39}^-. Chen et al. further considered doping of the B_{39}^- cage by Ca^{2+} to form $Ca@B_{39}^+$ endohedral borospherenes [66]. There appeared to be a family of borospherenes for mid-sized boron clusters, similar to the fullerene family. Large boron cages beyond B_{80} have also been considered computationally [62,67-74], but they are unlikely to be the global minimum on the potential energy surfaces.

A recent joint PES and computational study on B_{28}^- shows that its global minimum is a planar structure with C_2 symmetry with a low-lying seashell-like cage isomer also with C_2 symmetry [75]. Both are found to contribute to the observed photoelectron spectrum. In the neutral, the seashell C_2 cage is found to be the global minimum for the neutral B_{28}. Hence, the reverse of stability between the anion and neutral global minima in B_{28} is similar to that in B_{40} [33]. The B_{28}^- and B_{28} clusters are likely the smallest borosphenenes. It should be pointed out that there have been two recent computational studies on the 28-atom boron cluster: one reported the C_2 global minimum of the anion, but failed to find the C_2 seashell borospherene for the neutral [76], whereas another identified a seashell-like cage with C_1 symmetry for the neutral B_{28}, but did not locate the C_2 planar global minimum for the anion [77]. These reports again reflect the complexity of large boron clusters and the importance of careful global minimum searches and comparison with experiment, in order to obtain reliable structural information.

5. Concluding remarks and perspectives

Photoelectron spectroscopy of size-selected boron clusters in conjunction with computational chemistry has been a powerful approach to probe the structure and chemical bonding of size-selected boron clusters. Because of the complexity of boron clusters, comprehensive global minimum searches combined with high-level calculations, as well as comparisons with experimental data, are essential to ensure the true global minimum to be found for each cluster. Boron is known to be "a rule breaker", not only in its bulk forms, but also in the nanoscale. Even with the extensive experimental and theoretical efforts, no rules or construction principles can be

derived to predict the structures or growth of boron clusters. Each cluster has its own characteristics and requires the greatest care in global minimum searches and careful comparison with experimental data in order to make reliable conclusions about the most stable structures. In contrast to bulk boron, small boron clusters are all found to be planar or quasi-planar structures to accommodate their electron deficiency. The discovery of the planar hexagonal B_{36} cluster was a significant breakthrough in our understanding of boron clusters, providing indirect experimental evidence for the viability of borophenes. The subsequent syntheses of borophenes on silver substrates have provided macroscopic samples of this new form of 2D materials and will undoubtedly stimulate intense further investigations into their novel electronic and optical properties. The recent observations of transition metal doped 2D boron clusters [78,79] suggests the exciting possibility of metallo-borophenes [80]. The discovery of the first all-boron fullerene in B_{40}^- and B_{40} was also a major landmark in the study of boron clusters. There may be a family of borospherenes in the mid-size range, parallel to the fullerene family. These momentous findings have stimulated renewed interests in boron clusters and nanostructures. It is conceivable that the pace of discovery will continue to accelerate in boron clusters and more interesting structures and chemical bonds will be uncovered with increasing experimental and computational sophistication.

Acknowledgements. The experimental work on boron clusters at Brown University was supported by the National Science Foundation (Grant No. CHE-1263745). The author is grateful to his theoretical collaborators over more than a decade, including Prof. Alexander I. Boldyrev from Utah State University, Prof. Jun Li from Tsinghua University, Prof. Si-Dian Li from Shanxi University, and Prof. Xiao Chen Zeng from University of Nebraska-Lincoln. The author would also like to thank many current and former group members for their contributions, specifically, Dr. Hua-Jin Zhai, Dr. Constantin Romanescu, Dr. Wei Huang, Dr. Wei-Li Li, and Dr. Zachary Piazza.

References

[1] A. Gindulyte, W. N. Lipscomb, and N. L. Massa, Inorg. Chem. **37**, 6544-6545 (1998).

[2] I. Boustani and A. Quandt, Euro. Phys. Lett. **39**, 527-532 (1997).

[3] H. Tang and S. Ismail-Beigi, Phys. Rev. Lett. **99**, 115501 (2007).

[4] X. Yang, Y. Ding, and J. Ni, Phys. Rev. B **77**, 041402 (2008).

[5] N. G. Szwacki, A. Sadrzadeh, and B. I. Yakobson, Phys. Rev. Lett. **98,** 166804 (2007). [Erratum: Phys. Rev. Lett. **100**, 159901 (2008)]

[6] L. Hanley, J. L. Whitten, and S. L. Anderson, J. Phys. Chem. **92**, 5803-5812 (1988).

[7] S. A. Ruatta, L. Hanley, and S. L. Anderson, J. Chem. Phys. **91**, 226-239 (1989).

[8] P. A. Hintz, S. A. Ruatta, and S. L. Anderson, J. Chem. Phys. **92**, 292-303 (1990)

[9] P. A. Hintz, M. B. Sowa, S. A. Ruatta, and S. L. Anderson, J. Chem. Phys. **94**, 6446-6458 (1991)

[10] M. B. Sowa-Resat, J. S. Smolanoff, A. Lapicki, and S. L. Anderson, J. Chem. Phys. **106**, 9511-9522 (1997).

[11] H. J. Zhai, L. S. Wang, A. N. Alexandrova, and A. I. Boldyrev, J. Chem. Phys. **117**, 7917-7924 (2002).

[12] A. N. Alexandrova, A. I. Boldyrev, H. J. Zhai, L. S. Wang, E. Steiner, and P. W. Fowler, J. Phys. Chem. A **107**, 1359-1369 (2003).

[13] Z. H. Zhai, L. S. Wang, A. N. Alexandrova, A. I. Boldyrev, and V. G. Zakrzewski, J. Phys. Chem. A **107**, 9319-9328 (2003).

[14] H. J. Zhai, A. N. Alexandrova, K. A. Birch, A. I. Boldyrev, and L. S. Wang, Angew. Chem. Int. Ed. **42**, 6004-6008 (2003).

[15] H. J. Zhai, B. Kiran, J. Li, and L. S. Wang, Nature Mater. **2**, 827-833 (2003).

[16] A. N. Alexandrova, A. I. Boldyrev, H. J. Zhai, and L. S. Wang, J. Phys. Chem. A **108**, 3509-3517 (2004).

[17] B. Kiran, S. Bulusu, H. J. Zhai, S. Yoo, X. C. Zeng, and L. S. Wang, Proc. Natl. Acad. Sci. (USA) **102**, 961-964 (2005).

[18] A. N. Alexandrova, A. I. Boldyrev, H. J. Zhai, and L. S. Wang, Coord. Chem. Rev. **250**, 2811-2866 (2006).

[19] E. Oger, N. R. M. Crawford, R. Kelting, P. Weis, M. M. Kappes, and, R. Ahlrichs, Agew. Chem. Int. Ed. **46**, 8503-8506 (2007).

[20] A. P. Sergeeva, D. Yu. Zubarev, H. J. Zhai, A. I. Boldyrev, and L. S. Wang, J. Am. Chem. Soc. **130**, 7244-7246 (2008).

[21] W. Huang, A. P. Sergeeva, H. J. Zhai, B. B. Averkiev, L. S. Wang, and A. I. Boldyrev, Nature Chem. **2**, 202-206 (2010).

[22] A. P. Sergeeva, B. B. Averkiev, H. J. Zhai, A. I. Boldyrev, and L. S. Wang, J. Chem. Phys. **134**, 224304 (2011).

[23] Z. A. Piazza, W. L. Li, C. Romanescu, A. P. Sergeeva, L. S. Wang, and A. I. Boldyrev, J. Chem. Phys. **136**, 104310 (2012).

[24] A. P. Sergeeva, Z. A. Piazza, C. Romanescu, W. L. Li, A. I. Boldyrev, and L. S. Wang, J. Am. Chem. Soc. **134**, 18065-18073 (2012).

[25] I. A. Popov, Z. A. Piazza, W. L. Li, L. S. Wang, and A. I. Boldyrev, J. Chem. Phys. **139**, 144307 (2013).

[26] Z. A. Piazza, Ivan A. Popov, W. L. Li, R. Pal, X. C. Zeng, A. I. Boldyrev, and L. S. Wang, J. Chem. Phys. **141**, 034303 (2014).

[27] W. L. Li, R. Pal, Z. A. Piazza, X. C. Zeng, and L. S. Wang, J. Chem. Phys. **142**, 204305 (2015).

[28] L. S. Wang, Int. Rev. Phys. Chem. 35, in press (2016).

[29] A. P. Sergeeva, I. A. Popov, Z. A. Piazza, W. L. Li, C. Romanescu, L. S. Wang, and A. I. Boldyrev, Acc. Chem. Res. **47**, 1349-1358 (2014).

[30] D. Y. Zubarev and A. I. Boldyrev, J. Comput. Chem. **28**, 251-268 (2007).

[31] D. Y. Zubarev and A. I. Boldyrev, Phys. Chem. Chem. Phys. **10**, 5207-5217 (2007).

[32] Z. A. Piazza, H. S. Hu, W. L. Li, Y. F. Zhao, J. Li, and L. S. Wang, Nature Commun. **5**, 3113 (2014).

[33] H. J. Zhai, Y. F. Zhao, W. L. Li, Q. Chen, H. Bai, H. S. Hu, Z. A. Piazza, W. J. Tian, H. G. Lu, Y. B. Wu, Y. W. Mu, G. F. Wei, Z. P. Liu, J. Li, S. D. Li, and L. S. Wang, Nature Chem. **6**, 727-731 (2014).

[34] A. I. Boldyrev, and L. S. Wang, Phys. Chem. Chem. Phys. **18**, 11589-11605 (2016)..

[35] L. L. Pan, J. Li, and L. S. Wang, J. Chem. Phys. **129**, 024302 (2008).

[36] C. Romanescu, A. P. Sergeeva, W. L. Li, A. I. Boldyrev, and L. S. Wang, J. Am. Chem. Soc. **133**, 8646-8653 (2011).

[37] C. Romanescu, D. J. Harding, A. Fielicke, and L. S. Wang, J. Chem. Phys. **137**, 014317 (2012).

[38] A. Ricca and C. W. Bauschlicher Jr, Chem. Phys. Lett. **208**, 233-242 (1996).

[39] W. L. Li, Y. F. Zhao, H. S. Hu, J. Li, and L. S. Wang, Angew. Chem. Int. Ed. **53**, 5540-5545 (2014).

[40] W. L. Li, Q. Chen, W. J. Tian, H. Bai, Y. F. Zhao, H. S. Hu, J. Li, H. J. Zhai, S. D. Li, and L. S. Wang, J. Am. Chem. Soc. **136**, 12257-12260 (2014).

[41] Q. Chen, W. L. Li, Y. F. Zhao, S. Y. Zhang, H. S. Hu, H. Bai, H. R. Li, W. J. Tian, H. G. Lu, H. J. Zhai, S. D. Li, J. Li, and L. S. Wang, ACS Nano **9**, 754-760 (2015).

[42] I. Boustani, A. Quandt, E. Hernandez, and A. Rubio, J. Chem. Phys. **110**, 3176-3185 (1999).

[43] M. H. Evans, J. D. Joannopoulos, and S. T. Pantelides, Phys. Rev. B **72**, 045434 (2005).

[44] J. Kunstmann and A. Quandt, Phys. Rev. B **74**, 035413 (2006).

[45] K. C. Lau and R. Pandey, J. Phys. Chem. C **111**, 2906-2912 (2007).

[46] J. Kunstmann, V. Bezugly, H. Rabbel, M. H. Rummeli, and G. Cuniberti, Adv. Funct. Mat. **24**, 4127-4134 (2014).

[47] T. R. Gallev, Q. Chen, J. C. Guo, H. Bai, C. Q. Miao, J. G. Lu, A. P. Sergeeva, S. D. Li, and A. I. Boldyrev, Phys. Chem. Chem. Phys. **13**, 11575-11578 (2011).

[48] S. G. Xu, Y. J. Zhao, J. H. Liao, and X. B. Yang, J. Chem. Phys. **142**, 214307 (2015).

[49] A. B. Rahane and V. Kumar, Nanoscale **7**, 4055-4062 (2015).

[50] Y. Liu, E. S. Penev, and B. I. Yakobson, Angew. Chem. Int. Ed. **52**, 3156-3159 (2013).

[51] H. Liu, J. Gao, and J. Zhao, Sci. Rep. **3**, 3228 (2013).

[52] Z. Zhang, Y. Yang, G. Gao, and B. I. Yakobson, Angew. Chem. Int. Ed. **54**, 1-6 (2015).

[53] A. J. Mannix, X. F. Zhou, B. Kiraly, J. D. Wood, D. Alducin, B. D. Myers, X. Liu, B. L. Fisher, U. Santiago, J. R. Guest, M. J. Yacaman, A. Ponce, A. R. Oganov, M. C. Hersam, and N. P. Guisinger, Science **350**, 1513 (2015).

[54] B. Feng, J. Zhang, Q. Zhong, W. Li, H. Li, P. Cheng, S. Meng, L. Chen, and K. Wu, http://arxiv.org/abs/1512.05029.

[55] S. G. Xu, Y. J. Zhao, J. H. Liao, X. B. Yang, and H. Xu, http://arxiv.org/abs/1601.01393.

[56] E. S. Penev, S. Bhowmick, A. Sadrzadeh, and B. I. Yakobson, Nano Lett. **12**, 2441-2445 (2012).

[57] X. Wu, J. Dai, Y. Zhao, A. Zhuo, J. Yang, and X. C. Zeng, ACS Nano **6**, 7443-7453 (2012).

[58] C. Shang and Z. P. Liu, J. Chem. Theory Comput. **9**, 1838-1845 (2013).

[59] D. L. V. K. Prasad and E. D. Jemmis, Phys. Rev. Lett. **100,** 165504 (2008).

[60] H. Li, N. Shao, B. Shang, L. F. Yuan, J. Yang, and X. C. Zeng, Chem. Commu. **46**, 3878-3880 (2010).

[61] S. De, A. Willand, M. Amsler, P. Pochet, L. Genovese, S. Goedecker, Phys. Rev. Lett. **106,** 225502 (2011).

[62] F. Li, P. Jin, D. E. Jiang, L. Wang, S. B. Zhang, J. Zhao, and Z. Chen, J. Chem. Phys. **136,** 074302 (2012).

[63] H. W. Kroto, J. R. Heath, S. C. O'Brien, R. F. Curl, and R. E. Smalley, Nature **318**, 162-163 (1985).

[64] S. Goedecker, J. Chem. Phys. **120**, 9911-9917 (2004).

[65] Q. Chen, S. Y. Zhang, H. Bai, W. J. Tian, T. Gao, H. R. Li, C. Q. Miao, Y. W. Mu, H. G. Lu, H. J. Zhai, and S. D. Li, Angew. Chem. Int. Ed. **54**, 8160-8164 (2015).

[66] Q. Chen, T. Gao, W. J. Tian, H. Bai, S. Y. Zhang, H. R. Li, C. Q. Miao, Y. W. Mu, H. G. Lu, H. J. Zhai, and S. D. Li, Phys. Chem. Chem. Phys. **17**, 19690-19694 (2015).

[67] Q. B. Yan, X. L. Sheng, Q. R. Zheng, L. Z. Zhang, and G. Su, Phys. Rev. B **78**, 201401(R) (2008).

[68] N. G. Szwacki, Nanoscale Res. Lett. **3**, 49-54 (2008).

[69] R. R. Zope, T. Baruah, K. C. Lau, A. Y. Liu, M. R. Pederson, and B. I. Dunlap, Phys. Rev. B **79**, 161403(R) (2009).

[70] C. Ozdogan, S. Mukhopadhyay, W. Hayami, Z. B. Guvenc, R. Pandey, and I. Boustani, J. Phys. Chem. C **114**, 4362-4375 (2010).

[71] B. Shang, L. F. Yuan, X. C. Zeng, and J. Yang, J. Phys. Chem. A **114**, 2245-2249 (2010).

[72] J. T. Muya, G. Gopakumar, M. T. Nguyen, and A. Ceulemans, Phys. Chem. Chem. Phys. **13**, 7524-7533 (2011).

[73] R. R. Zope and T. Baruah, Chem. Phys. Lett. **501**, 193-196 (2011).

[74] P. A. Troshin, A. G. Avent, A. D. Darwish, N. Martsinovich, A. Abdul-Sada, J. M. Street, and R. Taylor, Science **309**, 278-281 (2005).

[75] Y. J. Wang, Y. F. Zhao, W. L. Li, T. Jian, Q. Chen, X. R. You, T. Ou, X. Y. Zhao, H. J. Zhai, S. D. Li, J. Li, and L. S. Wang, J. Chem. Phys. **144**, 064307 (2016).

[76] T. B. Tai and M. T. Nguyen, Phys. Chem. Chem. Phys. **17**, 13672-13679 (2015).

[77] J. Zhao, X. Huang, R. Shi, H. Liu, Y. Su, and R. B. King, Nanoscale **7**, 15086-15090 (2015).

[78] W. L. Li, T. Jian, X. Chen, T. T. Chen, G. V. Lopez, J. Li, and L. S. Wang, Angew. Chem. Int. Ed. **55**, 7358-7363 (2016).

[79] T. Jian, W. L. Li, X. Chen, T. T. Chen, G. V. Lopez, J. Li, and L. S. Wang, Chem. Sci., in press (2016).

[80] H. Zhang, Y. Li, J. Hou, K. Tu, and Z. Chen, J. Am. Chem. Soc. **138**, 5644-5651 (2016).

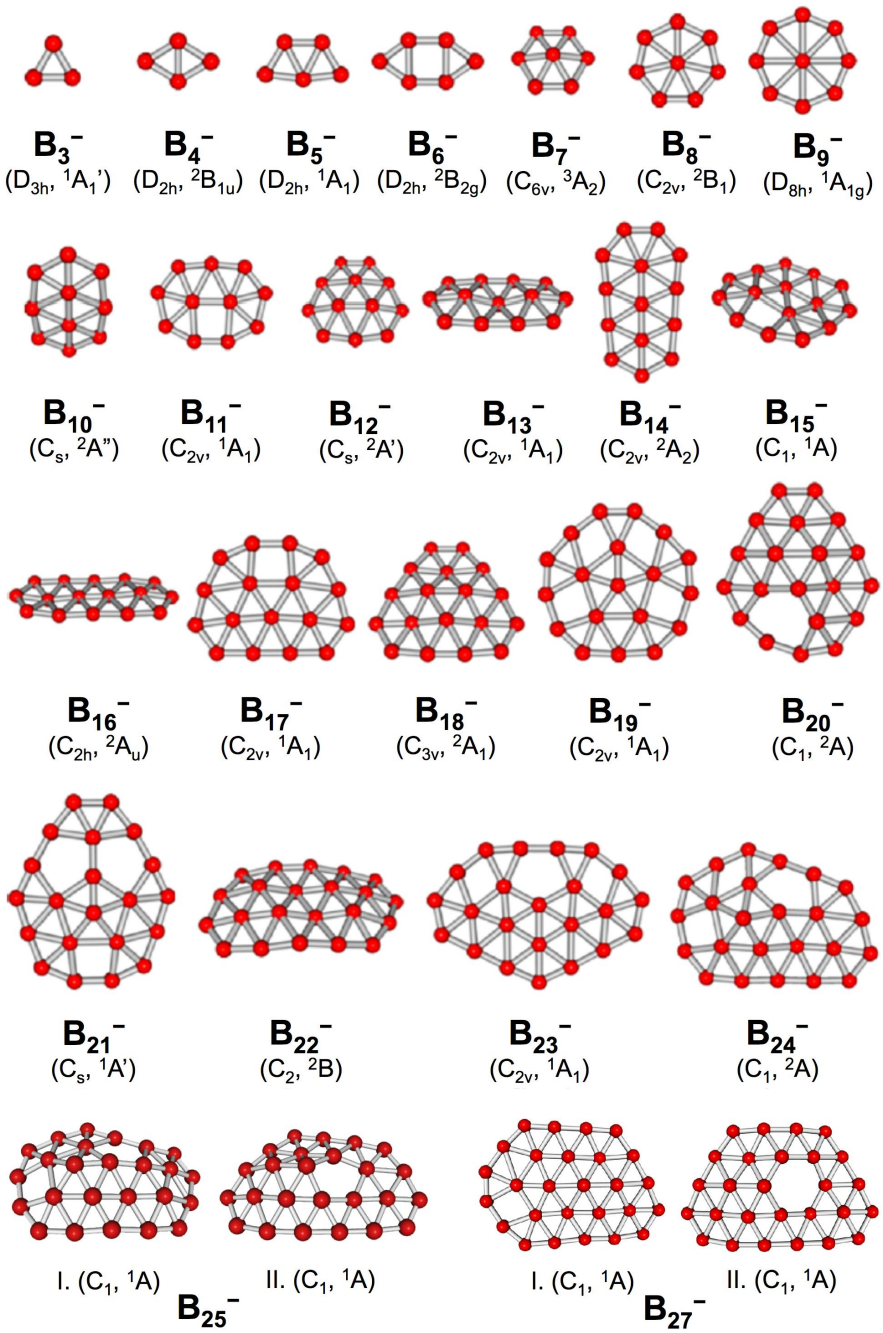

Figure 1. A summary of the global minima of B_n^- clusters (n = 3–25, 27) confirmed by experiment. Note that a close-lying isomer is also shown for B_{25}^- and B_{27}^-.

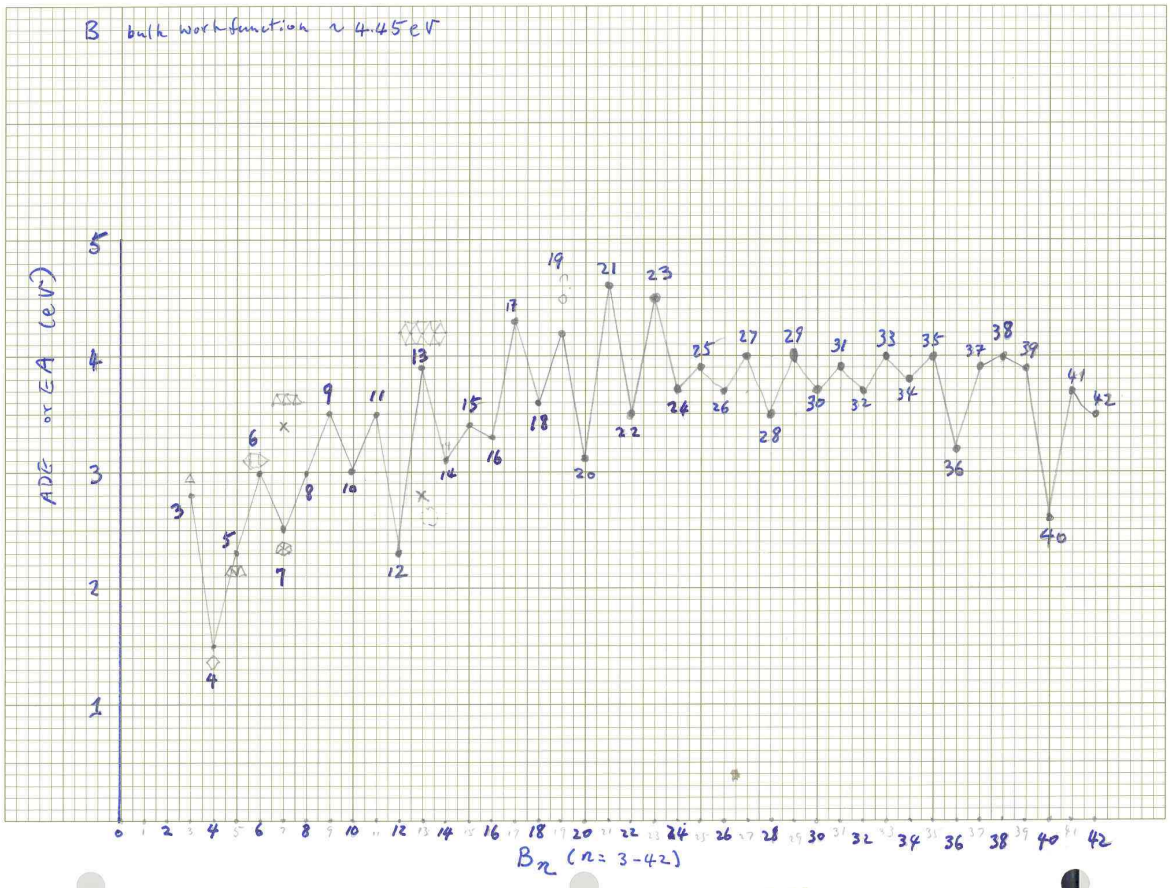

Figure 2. A preliminary manual plot of the electron affinity (EA) of B_n (n = 3–42) made in 2005 by the author.

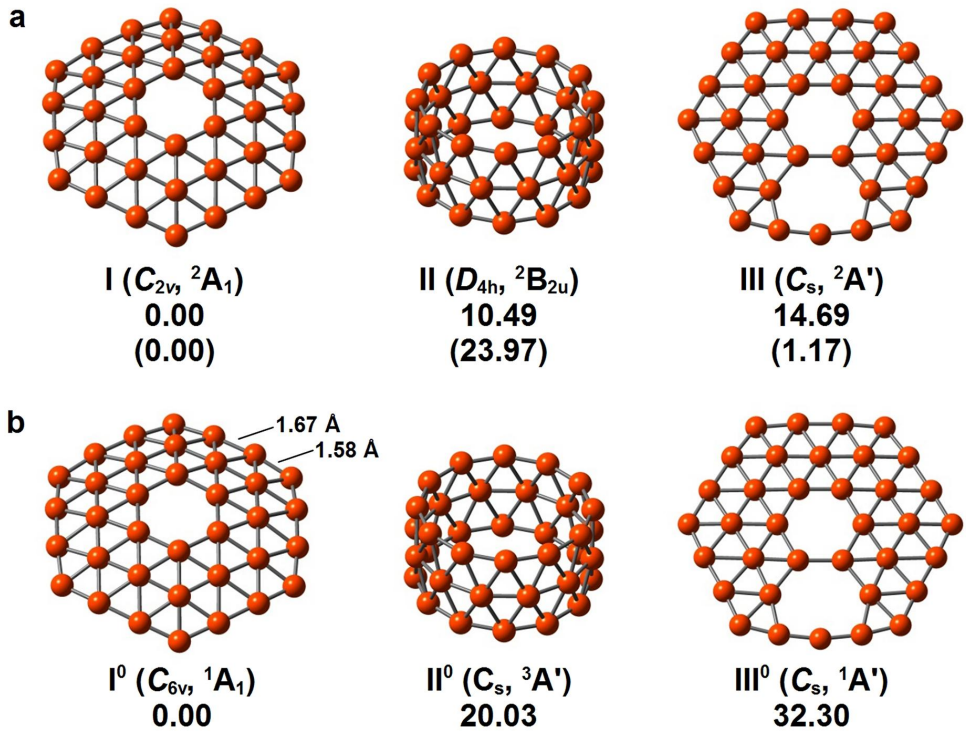

Figure 3. The global minimum and low-lying isomers of B_{36}^- (a) and B_{36} (b) [32].

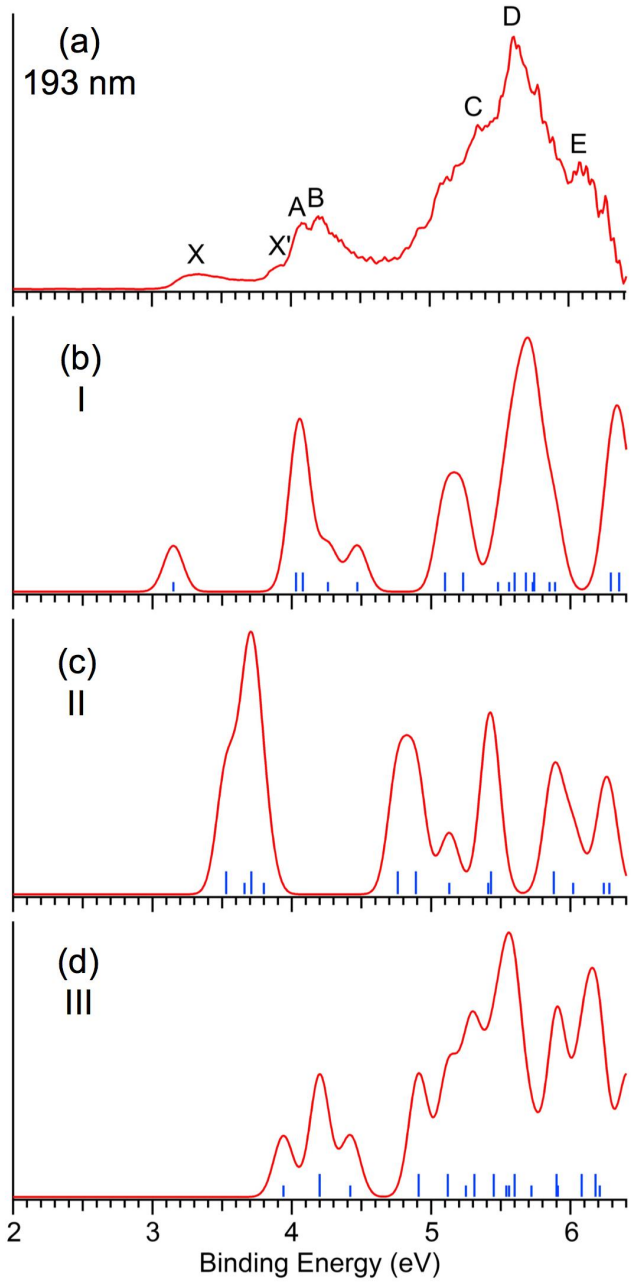

Figure 4. Comparison of the photoelectron spectrum of B_{36}^- (a) with simulated spectra from isomers I–III of B_{36}^- in Figure 4 [32].

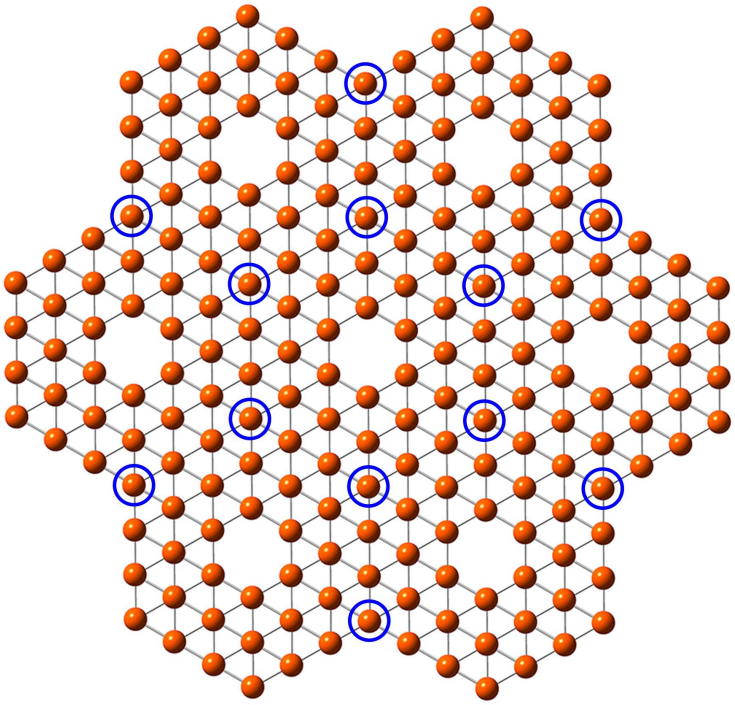

Figure 5. A schematic view of building up an atom-thin boron sheet with hexagonal holes or borophene using the hexagonal B_{36} by sharing one role of boron atoms between neighboring B_{36} units [32]. Removal of the circled atoms would result in the so-called α-sheet.

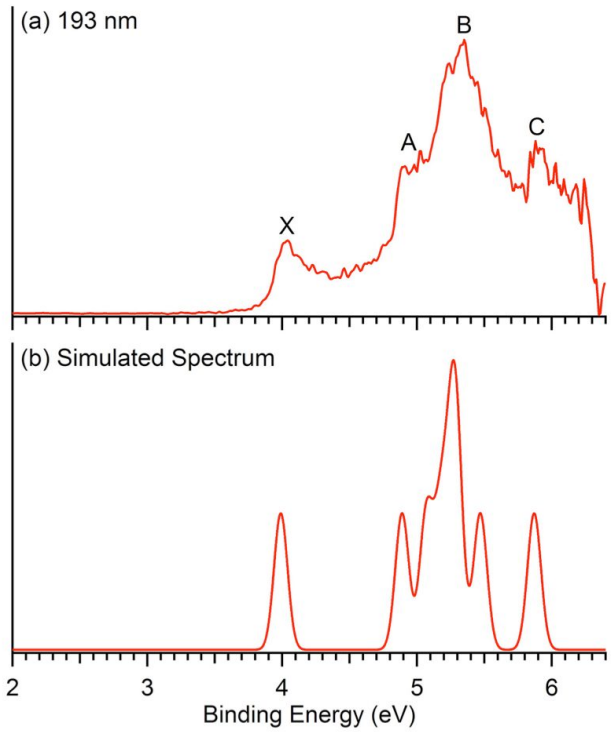

Figure 6. The photoelectron spectrum of B_{35}^- at 193 nm (a), compared with the simulated spectrum of the global minimum of B_{35}^- (Figure 7) [40].

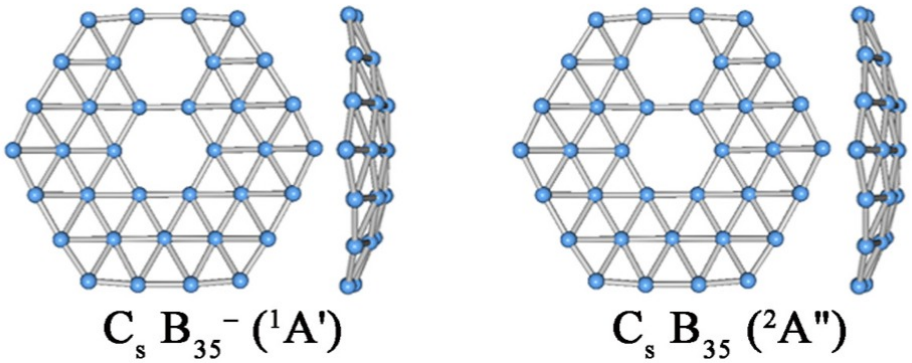

Figure 7. The global minimum of B_{35}^- and B_{35} [40].

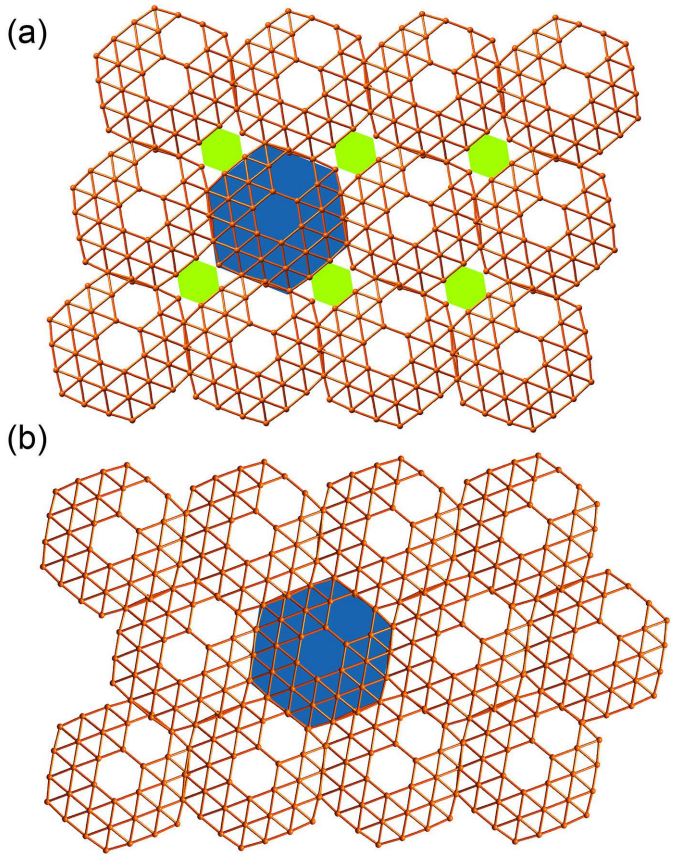

Figure 8. Schematics of building up borophenes with two different hexagonal hole patterns using the B_{35} units [40]. The blue shaded area represents a single B_{35} unit and the green area in (a) indicate monohexagonal holes created as a result of the arrangement of the B_{35} units.

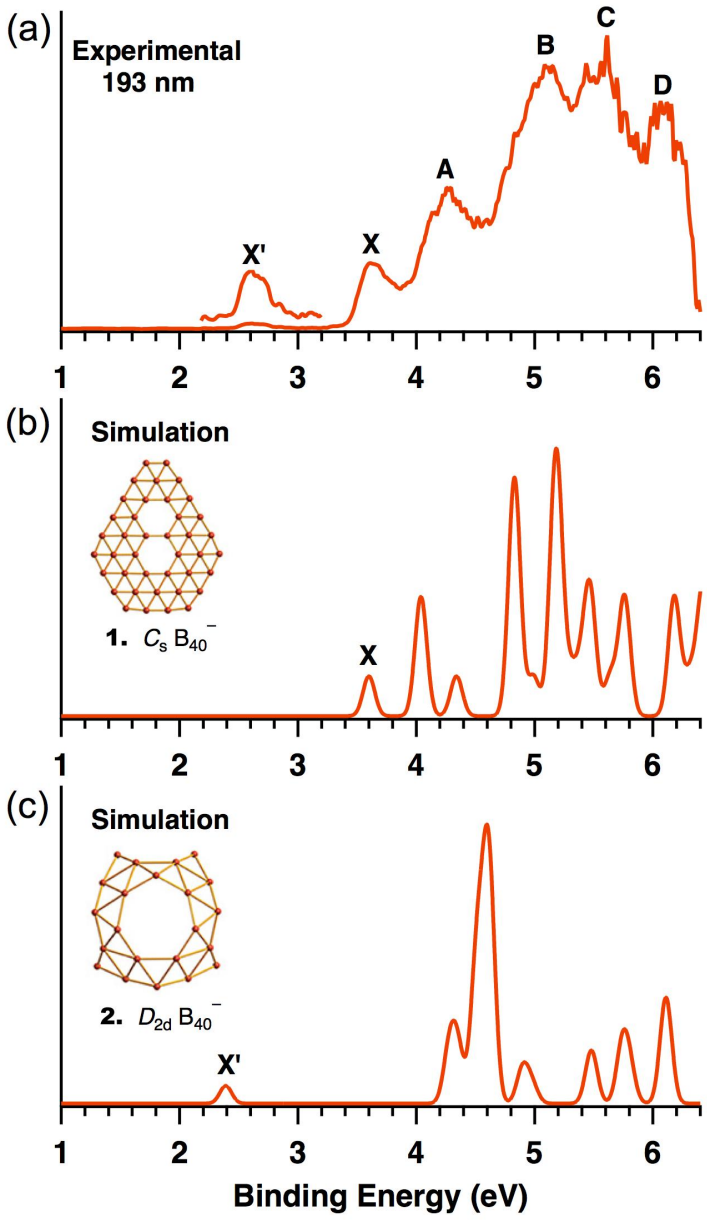

Figure 9. Comparison of the simulated spectra of the global minimum planar B_{40}^- (b) and the D_{2d} borospherene cage (c) with the experimental spectrum [33].

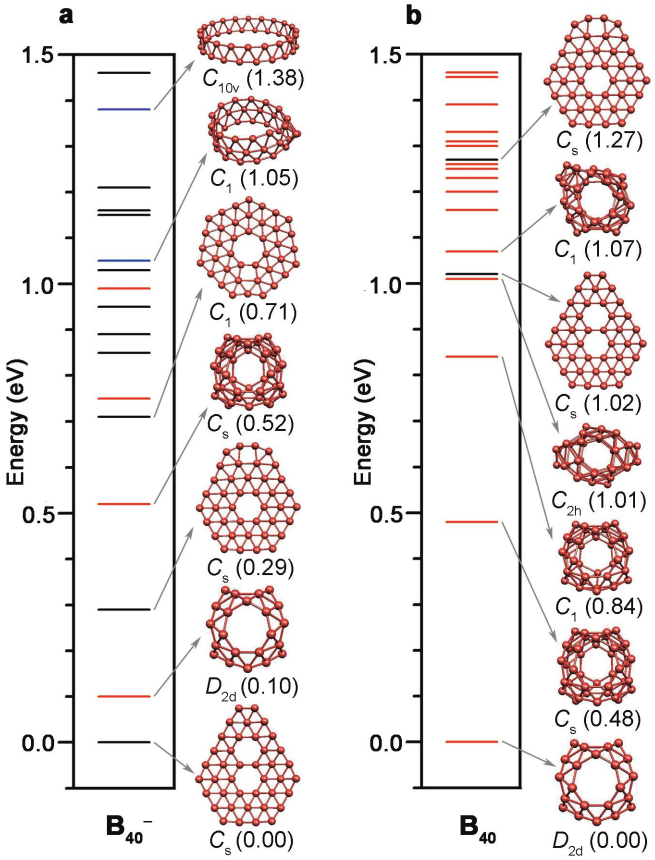

Figure 10. The configurational energy spectra of (a) B_{40}^- and (b) B_{40} at the PBE0 level of theory. The global minima and structures of selected isomers are shown [33]. Note the overwhelming stability of the D_{2d} cage for neutral B_{40}.

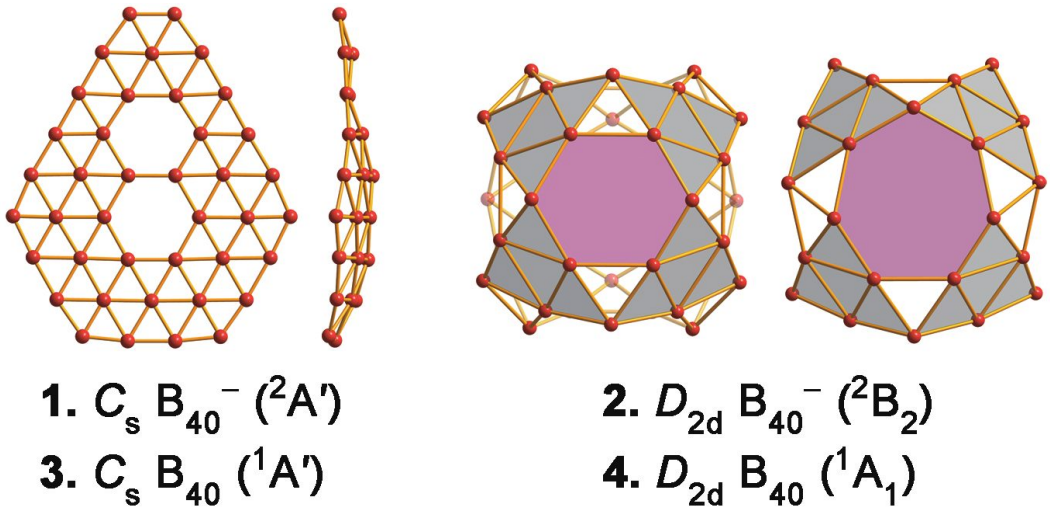

Figure 11. More detailed top and side views of the two lowest energy structures of B_{40}^- and the corresponding neutrals [33]. The shades in the cage structures were for easier viewing.

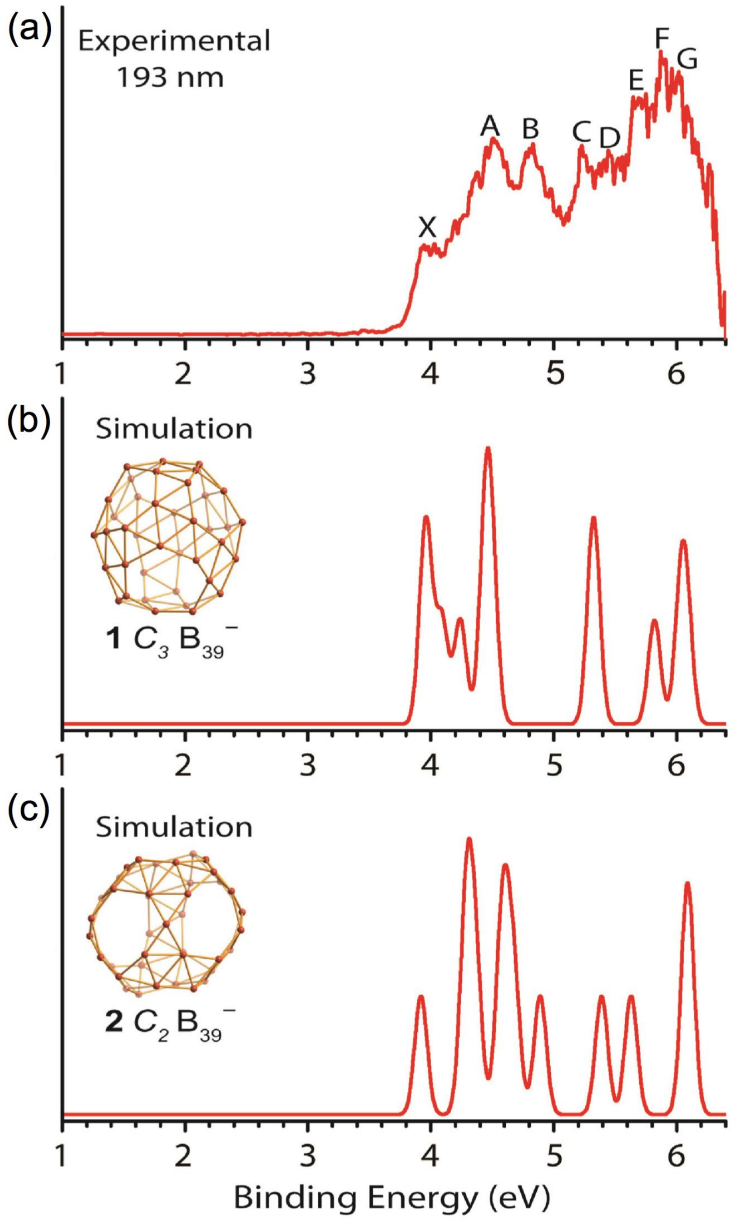

Figure 12. The photoelectron spectrum of B_{39}^- at 193 nm (a), compared with the simulated spectra of the C_3 global minimum of B_{39}^- (b) and its C_2 low-lying isomer (c) [41].

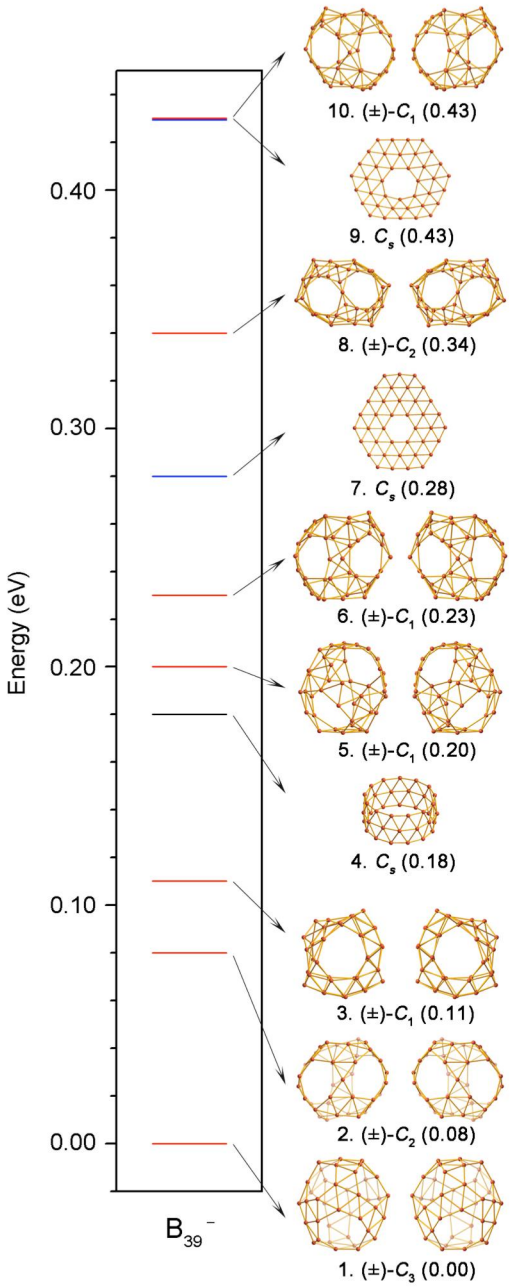

Figure 13. The global minimum and low-lying isomers of B_{39}^- within 0.45 eV of the global minimum [41].

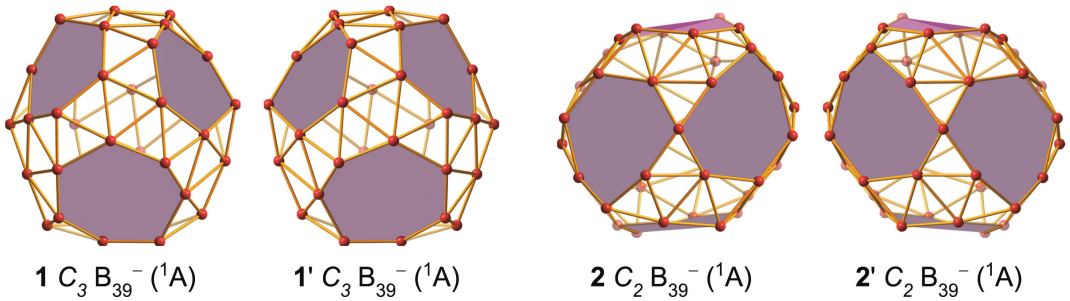

Figure 14. Detailed structures of the global minimum of the chiral C_3 B_{39}^-, its low-lying chiral C_2 isomer, and their respective enantiomers [41]. The shades are for easier viewing.